Thermal Degradation of Electroplated Nickel Thermal Microactuators

J. K. Luo, Y. Q. Fu, J. A. Williams, *Fellow, ASME*, and W. I. Milne

***Abstract*—In this paper, the thermal degradation of laterally operating thermal actuators made from electroplated nickel has been studied. The actuators investigated delivered a maximum displacement of ca. 20 μm at an average temperature of $\sim$450 °C, which is much lower than that of typical silicon-based microactuators. However, the magnitude of the displacement strongly depended on the frequency and voltage amplitude of the pulse signal applied. Back bending was observed at maximum temperatures as low as 240 °C. Both forward and backward displacements increase as the applied power was increased up to a value of 60 mW; further increases led to reductions in the magnitudes of both displacements. Scanning electron microscopy clearly showed that the nickel beams began to deform and change their shape at this critical power level. Compressive stress is responsible for nickel pileup, while tensile stresses, generated upon removing the current, are responsible for necking at the hottest section of the hot arm of the device. Energy dispersive X-ray diffraction analysis also revealed the severe oxidation of Ni structure induced by Joule heating. The combination of plastic deformation and oxidation was responsible for the observed thermal degradation. Results indicate that nickel thermal microactuators should be operated below 200 °C to avoid thermal degradation. [2009-0015]**

***Index Terms*—Back bending, electroplating, oxidation, plastic deformation, thermal actuator, thermal degradation.**

I. Introduction

THE ATTRACTION of microelectrothermal actuators for use in microsystems and microelectronics lies in the relatively large forces and displacements which they can generate [1]–[3]. With operational voltages comparable to those used in CMOS, they are particularly suitable for integration with electronic circuits for control and signal processing. In general, microactuators have longer lifetimes than their macro counterparts, owing to the reduced number of defects in components with such small linear dimensions. The operational durability and reliability of microactuators are thus generally superior to macroactuators. Microelectromechanical system (MEMS) switches and comb-drive structures based on electrostatic actuation have been operated up to tens of billion of cycles without failure [4]. However, thermal microactuators have shorter lifetimes, particularly when operated at high temperatures. When operated in these conditions, deterioration in actuation force and actuation frequency, as well as degradation in maximum displacement and catastrophic failure by burn-off or blowup, has been reported for both lateral and vertical thermal microactuators [5], [6]. Thermal degradation is attributable to both surface oxidation and plastic deformation caused by material creep at elevated temperatures. When a thermal microactuator is heated above some critical temperature, it may undergo localized material deformation, oxidation, creep, or even recrystallization in the most vulnerable position [5], [6]. In Si-based actuators, a structural deformation phenomenon, known as "back bending," is often observed, whereby the actuating elements will not return to their original positions once they have been "overactuated" but are left permanently bent or deformed in the direction opposite to that of normal actuation.

Plastic deformation caused by creep and recrystallization increases rapidly with temperature. For a typical lateral thermal actuator consisting of a combination of hot and cold arms, as shown in Fig. 1(a), the highest temperature occurs near the middle of the hot arm; however, the largest stress usually occurs either near the joint of the hot and cold arms or at the root of the beams or flexures which allow the structure to move. If material creep exists at a raised temperature, we should expect material pileup or accumulation to occur at the place where the compressive stress is the largest. Although there is no direct reported evidence of such compressive deformation, tensile tests of Si microbeams, at various elevated temperatures, have revealed thinning due to creep [7]. The temperature required for plastic deformation in a Si actuator is believed to be correlated with the intrinsic melting temperature ($\sim$1414 °C) of this material [8]. The observed plastic deformation transition temperature for Si actuators, however, is typically 600 °C $\sim$ 800 °C [6], which is much lower than the intrinsic melting temperature of silicon. It was believed that the plastic deformation of the silicon actuators is dominated by brittle-to-ductile transition temperature which is $\sim$660 °C [9], which is within the observed plastic deformation transition temperatures (600 °C $\sim$ 800 °C) for silicon thermal actuators. Although thermal degradation has been studied in microactuators for many years [5]–[11], the degradation mechanisms are still not clear.

Silicon is the dominant material used for MEMS devices not least because of the suite of microfabrication technologies and

Manuscript received January 15, 2009; revised September 15, 2009. First published November 18, 2009; current version published December 1, 2009. The work of J. K. Luo was supported in part by the Engineering and Physical Sciences Research Council under Project EP/D051266. Subject Editor M. Wong.

J. K. Luo was with the Engineering Department, University of Cambridge, CB3 0FA Cambridge, U.K. He is now with the Centre for Material Research and Innovation, University of Bolton, BL3 5AB Bolton, U.K. (e-mail: jl2@bolton.ac.uk.).

Y. Q. Fu was with the Engineering Department, University of Cambridge, CB3 0FA Cambridge, U.K. He is now with the Department of Mechanical Engineering, School of Engineering and Physical Sciences, Heriot-Watt University, EH14 4AS Edinburgh, U.K.

J. A. Williams and W. I. Milne are with the Engineering Department, University of Cambridge, CB3 0FA Cambridge, U.K.

Color versions of one or more of the figures in this paper are available online at http://ieeexplore.ieee.org.

Digital Object Identifier 10.1109/JMEMS.2009.2034394

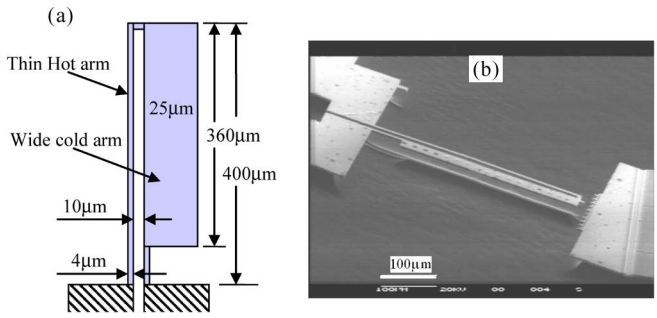

Fig. 1. (a) Schematic drawing of the U-shaped thermal microactuator. (b) SEM photograph of the U-shaped Ni thermal microactuator.

manufacturing facilities inherited from the microelectronics industry. Since metals have higher thermal expansion coefficients than silicon, metallic thermal microactuators have lower operation temperatures. For example, if a Si actuator needs an operation temperature around 1000 °C to deliver a particular displacement, then a Ni-based actuator would only require a temperature of ∼400 °C [12]. In addition, nickel-based actuators have much lower resistivity and are thus particularly suitable for microactuator-based microrelays and microswitches [13], [14].

Nickel and Ni–Fe alloys are the most studied metals for microactuators because of their attractive material properties and easy fabrication by electroplating [12], [13]. Although nickel has a high melting temperature (1455 °C), which is higher than that of silicon (1414 °C), it is ductile in nature. Metals oxidize at much lower temperatures than silicon, and thus, the temperature limitation of a metal device is expected to be much lower than its silicon counterpart. Indeed, a limiting temperature of ∼200 °C has been suggested for the nickel thermal actuators, although with little experimental support [15]. The degradation of electrodeposited Ni structures and devices has been studied under high stress by many groups, [16]–[18] but mostly at room temperatures. There is a lack of studies on Ni microstructures and devices under thermal stress. This paper reports a systematic investigation on the thermal degradation of a nickel thermal microactuator, including back bending, creep, and oxidation.

II. Fabrication and Electrical Testing

Fig. 1(a) shows a schematic drawing of the U-shaped lateral thermal actuator used for this investigation. Each device consisted of a thin hot arm and a wider cold arm joined by a thin flexure. All the U-shaped actuators used in this paper had the same dimensions. The length and width of the hot arms were 400 and 4 μm, respectively, with the corresponding dimensions of the cold arms being 360 and 25 μm. The flexure at the base of the cold arm was 40 μm long and 4 μm wide, and the gap between the hot and cold arms was 10 μm. When a current passes through a resistive device, its temperature rises through Joule heating. In the case of a thermoelectric actuator, the higher electrical resistance of the thinner beam leads to its reaching a much higher temperature than the cold arm. This, in turn, generates a greater change in length by thermal expansion, thus producing a deflection of the free tip laterally toward the cold arm.

The microactuators used in this paper were made from electroplated nickel films using a through-mask-plating technology [19], [20]. The devices were fabricated using a single-mask process on a 4-in Si wafer: The details of the process can be found in [12] and [21]. The thicknesses of the nickel films for two batches of devices, designated hereafter as D1 and D2, were 3 and 4 μm, respectively. The devices were released by etching the Si underneath the nickel beams using a SF_6 reactive ion etch process. The plasma etching conditions were as follows: a SF_6 flow rate of 45 sccm, a pressure of 150 mtorr, an RF power of 150 W, and an etch time of 15 min. The etch duration was long enough to remove all residual silicon from the back of the devices which were separated from the Si substrate by an air gap of 25–30 μm, and is sufficient to minimize conductive losses. Fig. 1(b) shows a scanning electron microscopy (SEM) of the D2 nickel microactuator with a Ni thickness of ∼4 μm. The surfaces of the devices were smooth with a typical roughness of less than 20 nm, and the sidewalls were almost vertical.

Electrical tests were conducted on the actuators using a probe station. The motion of the actuators was captured by a video camera with a resolution of 0.5 μm and was subsequently analyzed by a commercial software. The actuators were driven by a pulsed current using a Keithley voltage source Type 224, which simultaneously monitored the voltage drop across the devices, so that the power consumption and resistance of the actuator could be calculated. A rising temperature will increase the electrical resistance of the device due to the positive temperature coefficient of the resistivity of metals. The average temperature change of the thermal microactuator $\Delta T_{\rm ave}$ can be extracted from the change of the resistance by the relation [22]

$$\Delta T_{\rm ave} = T - T_0 = \left(R(T) - R_0\right)/R_0\xi \tag{1}$$

where T_0 is the room temperature, R_0 and $R(T)$ are the resistances of the device at room temperature and the raised temperature, respectively, and ξ is the temperature coefficient of the resistivity of the Ni with a value of 3×10^{-3} K^{-1} obtained from our previous work [23]. A metal such as nickel can be easily oxidized at high temperatures, so that the resistance of the actuator will increase during high-temperature measurements. This may cause an underestimation of the device temperature. Since significant metal oxidation occurs at temperatures > 450 °C, except for those specific experiments observing the enhanced deformation and oxidation processes, pulsed low currents were used for the measurements to keep the surface temperature of the beams at levels at which oxidation would be minimal.

The off-power tip position of a microactuator may gradually shift due to the so-called back-bending effect, and the resistance may also change after each measurement. In order to determine an accurate tip forward displacement and a back-bending displacement, it was necessary to measure both the off-power tip position (i.e., the back bent position) and resistance before starting each measurement. The measurement procedures were as follows: 1) measure the off-power position and resistance; 2) apply a pulse current; 3) measure the corresponding

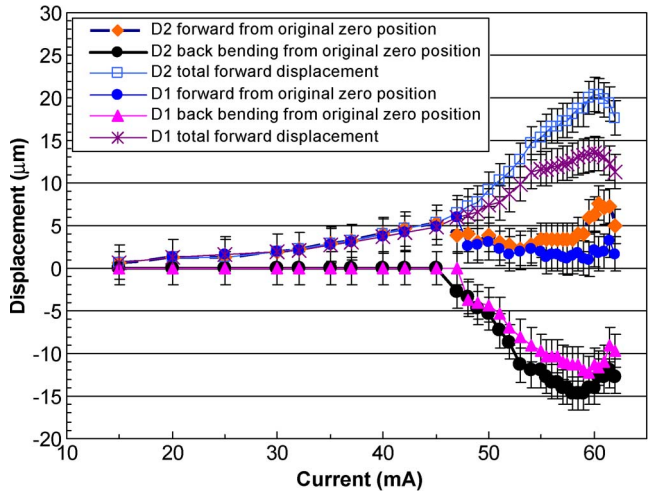

Fig. 2. Displacements of the Ni actuators as a function of pulsed current. The current pulsewidth was 0.1 s. Device D1 and D2 have different Ni thicknesses of 3 and 4 μm.

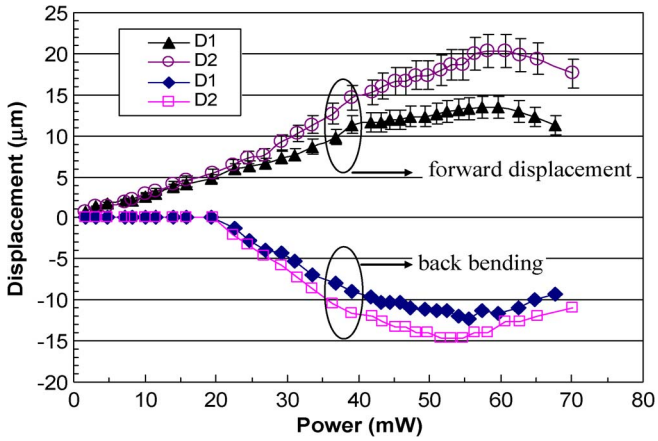

Fig. 3. Forward displacements and back bending of the Ni actuators as a function of power consumed, which were calculated from the current applied and voltage measured. The back bending appears at a current larger than 20 mA.

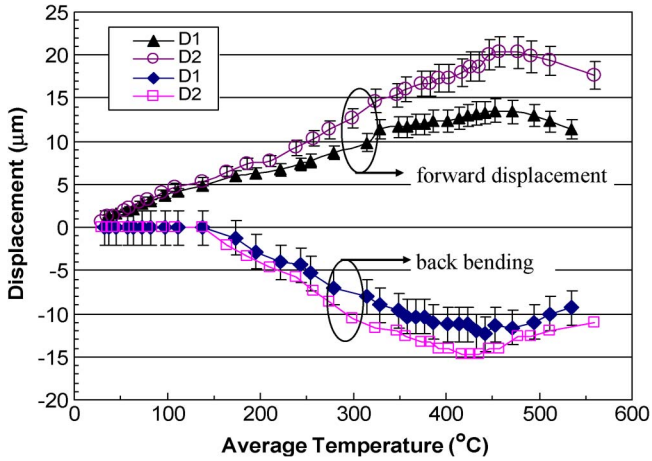

Fig. 4. Forward displacements and back bending as a function of average temperature extracted for two thermal actuators. The forward displacement is almost proportional to the average temperature. The back bending appears at an average temperature larger than 140 °C.

displacement and the voltage drop for resistance and power calculations; 4) turn off the current; and 5) remeasure the off-power position and resistance as part of the next measurement sequence. Metals have a positive temperature coefficient of resistivity, so that if the cooling of the hot arm is insufficient, then this element of positive feedback can lead to thermal runaway and structural failure. For the majority of the experiments, the current pulse duration was therefore limited to 0.1 s to avoid overheating and thermal destruction. However, in order to investigate the deformation and oxidation of the nickel beam that can occur in extreme circumstances, some experiments were carried out in which a current sufficient to generate the largest displacement of the actuator was applied to the actuator for a duration of 3 min. The subsequent surface morphology of the Ni beams was then characterized using field emission SEM (JEOL 6340F). Elemental concentrations at the surfaces of the nickel beams were measured using an energy dispersive X-ray (EDX) analyzer. The bonded oxygen content in the NiO_2 formed during operation could be calculated from the intensity of the EDX curves.

III. Results and Discussions

A. Displacement Versus Power

Two nickel thermal actuators D1 and D2 with nickel film thicknesses of 3 and 4 μm, respectively, were studied. Fig. 2 shows the observed displacement from the original zero position, back bending, and the total forward displacement, which is the sum of the former two, with current as input variable. Fig. 3 shows the back bending and the total forward displacement as a function of power calculated using the current applied and the resistance measured. The back-bending displacements were measured from the original zero position, and the minus sign represents its displacement opposite to the forward displacement. The total forward displacements (forward displacement in short hereinafter) of the thermal microactuator tips increased parabolically with the current applied and, up to an input of 60 mW, were roughly proportional to the applied power, in agreement with theoretical analysis in the literature [12], [22]. For both D1 and D2, the displacement of the tip reached a maximum at a power of 60 mW, specifically at values of $\sim$16 and 20 μm, respectively; beyond this, the displacement decreased with any further increase in power due to thermal degradation, as discussed later.

The observed forward displacement and back bending of the microactuators D1 and D2 are shown in Fig. 4 as a function of their average temperatures calculated by (1). The displacement is approximately proportional to the average temperature up to a value of 450°C, above which the displacement decreases. This may well be due to thermal degradation, as discussed later. For a similar displacement, a Si-based thermal actuator would typically require an average temperature of over 1000 °C [4], [5]. The much lower operating temperatures of nickel actuators are attributable to their larger thermal expansion coefficient $\alpha = 15 \times 10^{-6}$ K^{-1} compared to that of silicon for which $\alpha = 2.5 \times 10^{-6}$ K^{-1}.

The reported tip displacement for U-shaped actuators is typically $\sim$5% of the length of the hot arm [5]. The observed

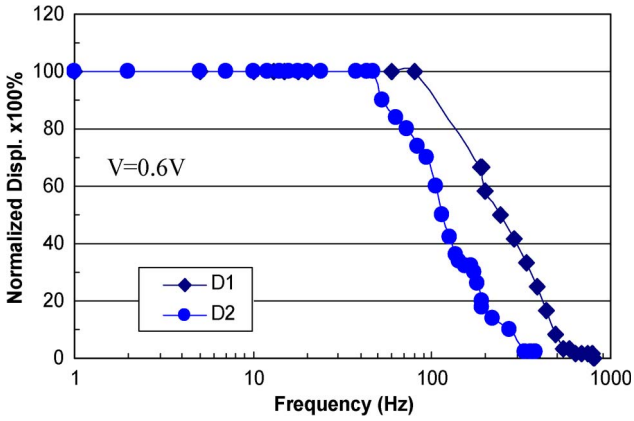

Fig. 5. Dependence of normalized displacements of Ni actuators on the frequency. The displacement remains unchanged at a frequency smaller than 40–100 Hz; it decreases with increasing the frequency and diminishes at a frequency higher than 300–700 Hz.

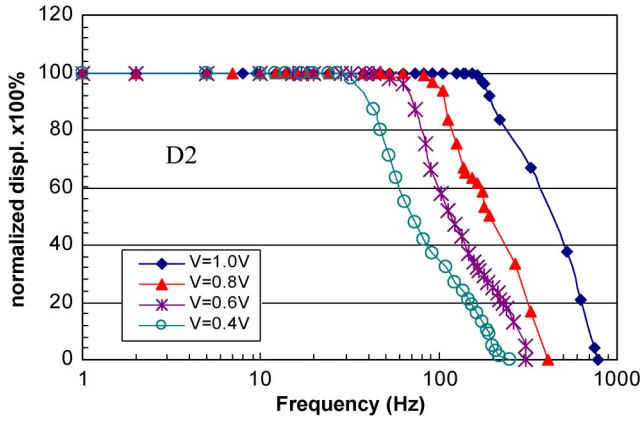

Fig. 6. Dependence of displacement on the frequency with peak voltage as a variable for device D2. It demonstrates that the cutoff frequency increases with increasing the voltage amplitude of the pulsed signal.

displacement of $\sim$20 μm for nickel devices with a length of 400 μm is therefore comparable to those reported for silicon actuators [1], [5] but occurs at a much low operating temperature. Further reductions in the temperature required or increases in the displacements of the tip might be achieved by either narrowing the gap between the hot and cold arms or by reducing the width of the hot arm further.

B. Frequency Dependence of Displacement

Square pulses with $t_{\rm on} = t_{\rm off}$ were used for experiments on the device dependence on frequency which was found to significantly influence the magnitude of the actuation that could be achieved. Fig. 5 shows the variation of the displacement, normalized by its maximum value, as a function of the driving frequency. As the frequency was increased from 1 Hz to values of ca. 50–100 Hz, the maximum observed displacement remained unchanged. However, with further increase in frequency, the tip displacement diminished, reducing gradually to zero when the frequency was on the order of 300–700 Hz.

The cooling processes of a U-shaped actuator of this scale will have time constants of between 1 and 10 ms [24], which are much greater than those associated with the Joule-heating process. Consequently, as the driving frequency is increased, cooling of the microactuator is suppressed, and the device will remain at an elevated temperature; hence, it is difficult for the actuator to deliver a significant displacement because of the small temperature difference between its hot and cold regions. The cutoff frequency of such a thermal actuator, defined as the frequency at which the effective displacement falls to zero, is thus determined mainly by the cooling process, which is a function of device dimensions and material properties [24]. For the devices used in these tests, the thermal cooling time constant based on the thermal conduction model through the bonding pads could be estimated, for example, using [24, eq. (9)], to be ca. 4 ms. This is comparable to those reported in [24] but rather more than those estimates of 0.5–0.2 ms made from the observed cutoff frequencies of several hundred Hertz. This difference might be attributable to an underestimation of heat loss through other mechanisms such as conduction or radiation through the air [25], [26].

The frequency dependence of the displacement is also significantly affected by the amplitude of the pulse voltage. Fig. 6 shows the dependence of the normalized displacement on frequency with voltage of the pulse as a variable. The cutoff frequency, as defined before, increases with the signal voltage. The reason for this behavior is not clear. The cooling process normally has an exponential relationship with time, i.e., cooling is faster at a high temperature. A higher temperature can be caused by a higher voltage pulse. Thus, a device with a high voltage pulse has a high cutoff frequency. The maximum temperature decreases when reducing the pulse voltage; thus, the cooling process becomes longer, and the cutoff frequency becomes smaller. Since the pulsewidth is much shorter than the 0.1 s used for the displacement measurements, the heating is not significant. However, a detailed observation revealed a back bending of up to 2 μm after the measurement at a signal voltage of 1.0V, indicating an average temperature rise of up to $\sim$200 °C, although this is much smaller than $T_a \sim 450$ °C, measured for the 0.1-s pulse measurement. The results imply that caution is needed in explaining the frequency dependence of microactuators.

C. Back Bending and Plastic Deformation

Fig. 7(a) and (b) shows the optical images of a thermal microactuator before and after applying a pulse current of 54 mA. It is apparent that the tip of the microactuator has become displaced from its original position by $\sim$15 μm in a direction opposite to that of the forward displacement, which is an example of the so-called back bending. Further increase in the current leads to blowup or burn-off near the middle of the hot arm, as shown in Fig. 7(c).

Figs. 2–4 also show the extent of back bending as a function of applied current, power, and average temperature for the two devices tested. Initially, there is no back bending, and then, the magnitude of the back-bending displacement increases with average temperature and falls away as the average temperature increases above 450 °C. Back bending occurs at an average temperature as low as $\sim$160 °C and reaches a

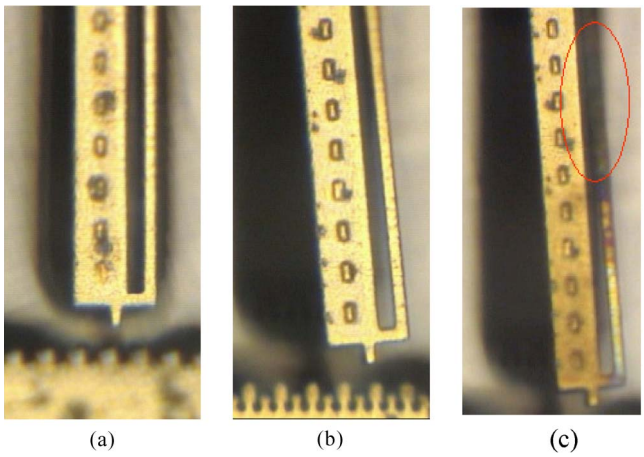

Fig. 7. Optical images of a thermal actuator show (a) the initial tip position and (b) the back bending after applying a pulse current of 54 mA and (c) burn-off followed by a high current of ∼62 mA.

maximum backward displacement of 15 μm at ~ 450 °C, which is ∼75% of the total forward displacement. The observed back-bending behavior with temperature for the D1 and D2 nickel microactuators is significantly different from those reported for silicon microactuators [6]. First, the average temperature of ~ 160 °C, which induces a measurable back bending for the nickel microactuators, is much lower than that of ~ 660 °C for the Si-based thermal actuators [6]. Second, while the back-bending displacement of the silicon actuators increases with power initially, it then remains at the maximum value as the power is further increased until the hot arm blows up [6]. Silicon is a relatively brittle material with a high melting temperature, which can easily fracture or cleave along grain boundaries rather than softening at large stresses and high temperature. Further increases in temperature have been observed to lead to significant recrystallization and abnormal grain growth for polysilicon-based thermal actuators [10], [11]. Polysilicon recrystallization to form large grain structures with crystal facets was observed at a temperature of 1100 °C, which, while much lower than the melting temperature, roughly coincides with the temperature at which significant creep might be expected [9], [10]. Under a tensile stress at a high temperature, silicon plastic deformation is characterized by grain boundary separation, internal cracking, and the formation of cavities [6], [10], rather than ductile necking.

Although nickel has a comparable melting temperature to silicon, it is ductile. The temperature to initiate plastic deformation in the nickel-based thermal actuators is much lower than that of comparable silicon microactuators. Since the estimated maximum temperature of the beam is ~ 680 °C, deformation by creep would seem to be responsible for the significant back-bending behavior of the nickel beams. Creep is thermally activated, so that both stress and temperature have profound effects on the process. Creep in metals can occur even at room temperature, provided that the stress level is sufficiently high [27]–[29]. This is significantly different from that of the silicon thermal actuators. As maximum temperature rises, the stress required to introduce creep in a nickel thermal actuator is much lower than that of a silicon actuator. Metals become much more reactive at high temperatures, and metallic surfaces will be oxidized quickly at relatively low temperatures. However, the oxidation of surface seems unlikely to be instrumental in reducing the length of the hot arm as the volume of the material normally increases after oxidation, and so is unlikely to be the cause of the back bending of the nickel device.

The temperatures shown in Fig. 4 are the averages extracted from the variation of the resistances of the nickel microactuators D2. The maximum temperature is near the middle of the hot arm. A previous analysis based on the thermal conduction model indicated that the maximum temperature increase of the hot arm $\Delta T_{\max}$ would be expected to be about 1.5 times the calculated average temperature increase ΔT_{ave} [21], [22]. Assuming an ambient temperature of 20 °C, the average temperature of 160 °C shown in Fig. 4 corresponds to a maximum temperature of $\sim 1.5 \times (160-20) + 20 = 230$ °C, i.e., close to 220 °C suggested by Lee *et al.* [15]. The estimated average temperature of 450 °C for severe degradation corresponds to a maximum temperature of ~ 665 °C, which should be high enough to induce significant creep, particularly at a large compressive stress. Furthermore, it is possible that these figures for average and maximum temperatures are underestimates as a result of the simplified model. The actual maximum temperature might exceed that estimated by ∼20%.

Device D1 showed smaller displacements in both forward displacement and back bending than those of the device D2, as shown in Figs. 2–4. It is believed to be caused by the thin Ni film, which is 3 μm. When the film thickness is smaller than the width of the hot arm, a certain degree of out-of-plane buckling under thermal stress occurs. This will not introduce a plastic deformation, as it is well within the elastic state, but reduce the forward displacement and back bending.

In order to investigate the cause of back bending, the nickel microactuators were thermally stressed by passing a high current of 54 mA through the structure for 3 min, and the resulting changes in beam morphology were studied. The 54-mA current chosen for the experiment corresponds to the near-worst case of the back bending, as shown in Fig. 2. However, the average temperature for this experiment should be higher than that at 54 mA shown in Fig. 4, as the device was heated for 3 min, which is much longer than the 0.1-s pulse measurement. The temperature increases, owing to the positive temperature coefficiency of the resistivity. At the end of 3 min, the average temperature raised from ~ 450 °C to ~ 500 °C, calculated from the increased resistance, corresponding to a maximum temperature of $\sim 1.5 \times (500-20) + 20 = 740$ °C. Fig. 8 shows the SEM images of a hot arm at various locations along its length after such a thermal treatment which illustrates some significant changes. Near the tip joint with the cold arm, the hot arm has retained the smooth surface finish of the original. At some distance from its ends, the surface of the hot arm becomes rougher and more rounded—evidence of plastic flow. Toward its mid-length, the beam cross section is significantly thinner, exhibiting a discernable neck. Near this position, on both sides of it, there is a significant accumulation or pileup of material. These changes in section, the general rounded appearance and lack of any preferred crystal facet, indicate that the metal has undergone a reflow process. As the melting temperature of nickel is 1455 °C, it is unlikely that the reflow is caused by

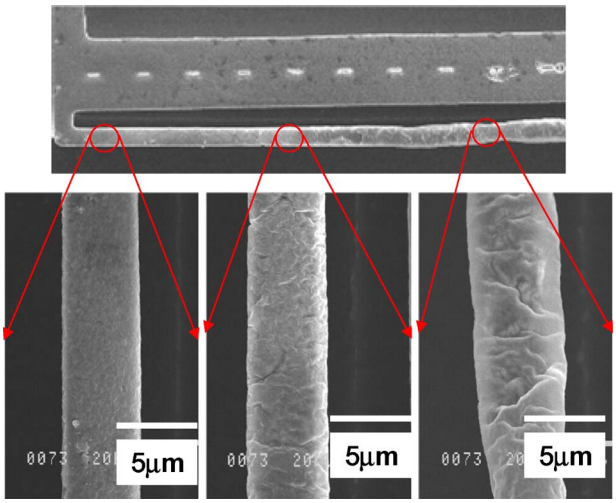

Fig. 8. SEM photographs of the hot arm in different places. The device had undergone heating by a current of 55 mA for 3 min. It showed the Ni pileup near the hotter places and necking at the hottest spot.

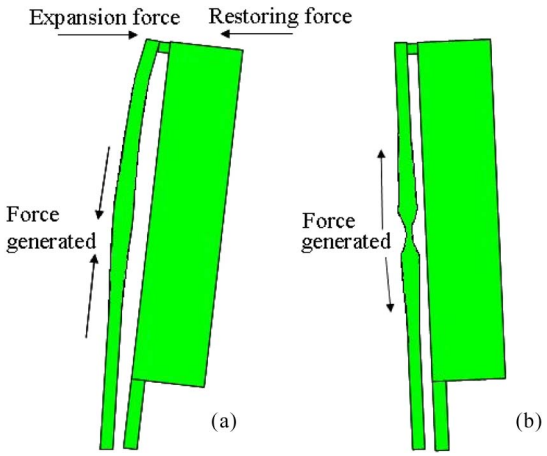

Fig. 9. (a) Schematic drawing of force acting on the hot arm when the current is applied; restoring force produces a compressive stress, leading to pileup of Ni. (b) When the current is removed, restoring force produces a tensile stress, leading to necking of the hot arm.

melting. It is believed that the material pileup and reflow are associated with creep encouraged by elevated temperatures and high stresses.

A dynamic model can thus be proposed for the plastic deformation of the nickel thermal microactuator shown schematically in Fig. 9. When the current is first applied, the differential Joule heating of the thinner arm causes it to become hotter, and thus, in an attempt to thermally lengthen by a greater margin than the adjacent cold arm, this puts the material under a compressive load. This compressive stress causes the material to deform and pile up in compression, the raised temperature accelerating this process. Nickel accumulates near the hottest section forming the comparatively large folded structures visible at this section of the beam. It is this effective shortening of the hot arm that is responsible for the subsequent back bending of the actuator. Upon removing the current, the beam rotates about its base as the force in the thinner arm changes from compressive stress to tensile stress. This tensile stress tends to elongate the shortened arm. Since the middle hottest section is

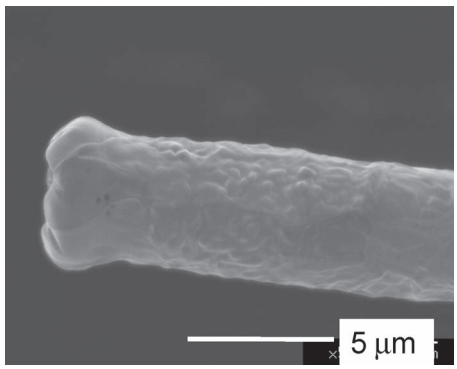

Fig. 10. SEM photograph of a blowup tip, showing a rounded structure which was caused by thermal runaway and melting.

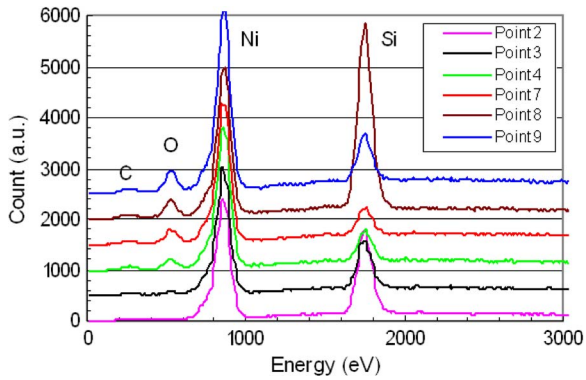

Fig. 11. EDX spectra from the surface of a hot arm after thermal stress at 55 mA for 3 min. As approaching the middle of the arm, the oxygen signal becomes much stronger.

the mechanically weakest, it is here that the extension occurs, manifesting itself as the observed neck.

It is thus the combination of pileup and necking that is believed to be responsible for the decreases in forward and back-bending displacements at $T_{\rm ave} = T_0 + \Delta T_{\rm ave} => 450\ ^\circ$C, as shown in Fig. 4. At a modest temperature, material pileup leads to the shortening of the arm, causing the back bending and reduction of forward displacement upon removing the current. At $T_{\rm ave}$ higher than 450 °C, necking prevents further shortening of the arm; hence, the back-bending displacement decreases as the temperature increases further. Any further increase in the current increases the temperature rapidly principally because of the positive temperature coefficient of the resistivity of nickel, rapidly leading to blowup of the hot arm. Fig. 10 shows a SEM image of the tip of a failed arm, clearly showing the rounded reflow structure.

D. Thermal Oxidation of the Beam

The surface of the nickel beams can be easily oxidized in air at high temperatures, and this may significantly affect the performance of these thermal actuators as a result of gradual changes in their resistance and mechanical properties. EDX was used to characterize the element concentration along the hot arm of the device shown in Fig. 8, and the results are shown in Fig. 11. Point 2 corresponds to a position where the hot and cold arms are linked, and point 9 is close to the neck; intermediate

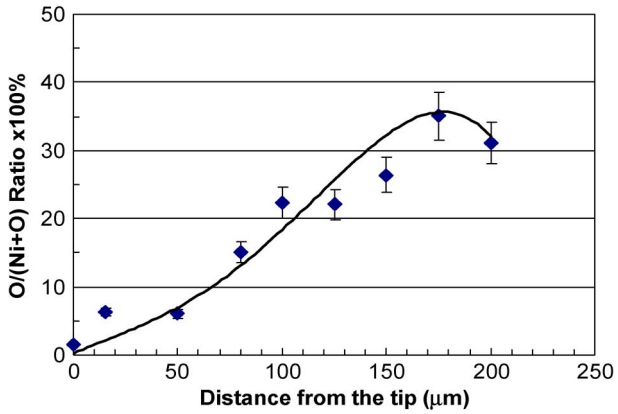

Fig. 12. Distribution of oxygen to Ni ratio along the hot arm. The oxygen content reaches the highest level at the middle of the hot arm.

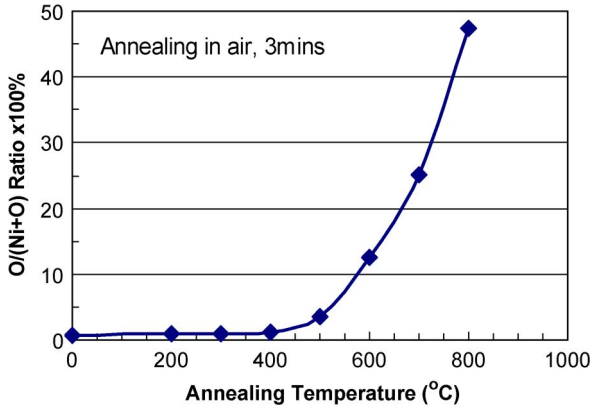

Fig. 13. Oxygen to nitrogen ratio as a function of annealing temperature for a Ni metal annealed in air for 3 min. The oxygen concentration increases rapidly as the temperature is over 450 °C and reaches ∼36% at ∼750 °C.

points are close to being equally spaced between them. The Si signal is from the silicon substrate, as the scanning area of the EDX measurements is wider than the hot arm width. Nickel is the dominant peak with a small trace of carbon, which is probably the residue from photoresist and plasma etching gases, as well as some carbon absorbance from the ambient. The oxygen concentration on the surface of the wide arm is typically at the level of $< 2\%$ (near the detection limitation) and is attributed to the thin native oxide and oxygen absorbance from the ambient. Fig. 12 shows the oxygen concentration results along the hot arm after the thermal overload treatment. The oxygen concentration increases steadily from the arm edge and reaches its highest value of ca. 36% roughly at the middle of the hot arm. This clearly indicates that most of the hot arm surface is oxidized after treatment with a 54-mA current maintained for 3 min. The profile of the oxygen concentration along the hot arm is also similar to the temperature profile obtained by finite-element-analysis-based modeling [3], [25], implying that the high temperature is directly responsible for the observed oxidation.

For comparison, a series of electroplated Ni samples were also annealed at temperatures from 200 °C to 800 °C for 3 min in an air furnace (rapid thermal annealing), and their oxygen concentration similarly investigated by EDX. The results are shown in Fig. 13 as a function of the annealing temperature. Up to 400 °C, the oxygen concentration remains below the detection limitation but grows rapidly as the temperature increases above 400 °C. The comparison of $\mathrm{O}/(\mathrm{O}+\mathrm{Ni})$ ratios along the hot arm of the actuator with those of the annealed samples implies that the highest temperature of the hot arm was around ∼760 °C, which is in good agreement with the estimated maximum temperature of 740 °C from the thermal conduction model discussed before.

We also observed that the electrical resistance of the actuator could be changed by the application of a current-driven thermal cycle. This is illustrated by the data of Fig. 14 which shows how the resistance of the device, measured at room temperature, was influenced by the calculated average temperature during the imposed thermal cycle. The resistance was measured at room temperature by allowing the actuator to cool down prior to each measurement, while the average temperature was calculated

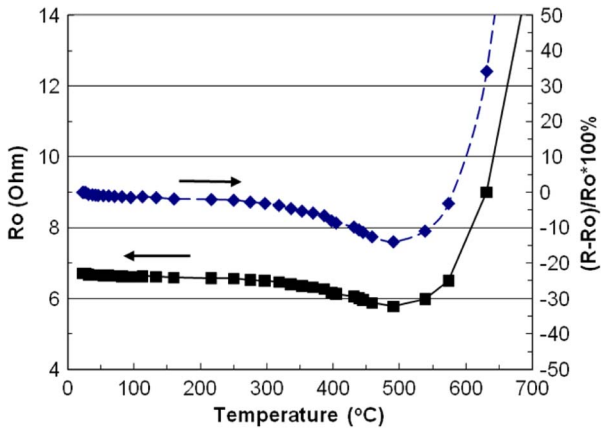

Fig. 14. Resistance of the thermal actuator as a function of average temperature measured. The resistance initially decreases, owing to annealing, and then increases rapidly when temperature exceeds 500 °C due to surface oxidation.

using the resistance measured when the current was on. As the current increases, the average temperature rises. The resistance of the device, determined principally by that of the hot arm, initially slowly decreased with increasing temperatures up to a value of ca. 500 °C, above which the resistance increased rapidly, leading to thermal runaway and blowup. The initial fall of the resistance with increasing average temperature is believed to be caused by an annealing effect. Upon annealing at a modest temperature, an electroplated nickel structure normally becomes dense with an increase in grain size and a fall in resistance [30], [31]. Any further increase in average temperature leads to severe surface oxidation, thus increasing the resistance until the current path fails. The observed onset temperature of ∼500 °C for the resistance to increase rapidly coincides with that of $\mathrm{O}/(\mathrm{Ni}+\mathrm{O})$ ratio versus temperature profile shown in Fig. 13. It is also clear that the resistance increases dramatically after $T_{\mathrm{ave}} \geq 500$ °C and reaches more than 150% of its ambient value at 700 °C, at which the actuators become sufficiently degraded to lead to a decreased displacement. It can be concluded that both creep and the surface oxidation at raised temperatures are responsible for the degradation in displacement of the nickel thermal actuators.

IV. Summary

U-shaped thermal microactuators were fabricated by a single-mask process using electroplated nickel as the active material. Their displacement and back bending have been characterized, and thermal degradation has been investigated in detail. The results can be summarized as follows.

1) The nickel thermal actuators investigated delivered displacements of up to 20 μm at an average temperature of 450 °C, which is much lower than those generally required by Si-based microactuators. The displacement strongly depends on the voltage amplitude of the pulse signal used. The typical cutoff frequency for the thermal actuators with a length of 400 μm was between 300 and 1000 Hz.
2) The phenomenon of back bending has been observed in the chosen nickel-based thermal microactuators becoming evident at average temperatures as low as 160 °C: This corresponds to a maximum temperature of 240 °C in the hot beam. These values are much lower than what would be expected in the case of silicon-based microactuators.
3) The magnitudes of both forward and back-bending displacements have become larger with increases in temperature up to 450 °C, but then have been subsequently decreased with temperature. Plastic deformation at high temperature and surface oxidation of the nickel hot arm are responsible for this phenomenon.
4) Reflow of the nickel has occurred under a compressive stress at raised temperatures, which can cause the material to pile up and thus make the beam locally larger in cross section. Conversely, a tensile stress generated upon the removal of the current can cause necking and local thinning of the hot arm.
5) EDX characterization has revealed that the surface of the hot arm is almost fully oxidized at a temperature of $\sim$750 °C, leading to a rapid increase of the resistance of the overall device.
6) Both plastic deformation and surface oxidation at raised temperatures have been responsible for the reduction in the available displacement of thermal actuators.

References

[1] J. R. Reid, V. M. Bright, and J. H. Comtois, "Force measurements of polysilicon thermal micro-actuators," *Proc. SPIE*, vol. 2882, pp. 296–306, 1996.

[2] T. Moulton and G. K. Ananthasuresh, "Micromechanical devices with embedded electro-thermal-compliant actuation," *Sens. Actuators A, Phys.*, vol. 90, no. 1/2, pp. 38–48, May 2001.

[3] Q. A. Huang and N. K. Lee, "Analysis and design of polysilicon thermal flexure actuator," *J. Micromech. Microeng.*, vol. 9, no. 1, pp. 64–70, Mar. 1999.

[4] R. L. Borwick, P. A. Stupar, and J. DeNatale, "A hybrid approach to low-voltage MEMS switches," in *Proc. 12th Int. Conf. Transducer, Solid-State Sens., Actuators Microsyst.*, 2003, vol. 1, pp. 859–862.

[5] J. H. Comtois and V. M. Bright, "Applications for surface-micromachined polysilicon thermal actuators and arrays," *Sens. Actuators A, Phys.*, vol. 58, no. 1, pp. 19–25, Jan. 1997.

[6] S. Deladi, G. Krijnen, and M. Elwenspoek, "Distinction of the irreversible and reversible actuation regions of B-doped poly-Si based electrothermal actuators," *J. Micromech. Microeng.*, vol. 14, no. 9, pp. S31–S36, Sep. 2004.

[7] J. Bagdahn and W. N. Sharp, "Fracture strength of polysilicon at stress concentration," *J. Microelectromech. Syst.*, vol. 12, no. 3, pp. 302–312, Jun. 2003.

[8] J. M. Maloney, D. S. Schreiber, and D. L. DeVoe, "Large-force electrothermal liner micromotors," *J. Micromech. Microeng.*, vol. 14, no. 2, pp. 226–234, Feb. 2004.

[9] R. A. Conant and R. S. Muller, "Cyclic fatigue testing of surface-micromachined thermal actuators," in *Proc. Amer. Soc. Mech. Eng.*, 1998, vol. DSC-V.66, pp. 273–277.

[10] S. Nakao, T. Ando, M. Shikeda, and K. Sato, "Mechanical properties of a micron-sized SCS film in a high-temperature environment," *J. Micromech. Microeng.*, vol. 16, no. 4, pp. 715–720, Apr. 2006.

[11] A. Tuck, A. Jungen, A. Geisberger, M. Ellis, and G. Skidmore, "A study of creep in polysilicon MEMS devices," *J. Eng. Mater. Technol.*, vol. 127, no. 1, pp. 90–96, Jan. 2005.

[12] J. K. Luo, J. H. He, A. J. Flewitt, D. F. Moore, S. M. Spearing, N. A. Fleck, and W. I. Milne, "Development of all metal electro-thermal actuators and its applications," *J. Microlith. Microfab. Microsyst.*, vol. 4, no. 2, p. 023012-1, 2005.

[13] P. M. Zavracky, S. Majumder, and N. E. McGruer, "Micromechanical switches fabricated using nickel surface micromachining," *J. Microelectromech. Syst.*, vol. 6, no. 1, pp. 3–9, Mar. 1997.

[14] I. Schiele, J. Huber, B. Hillerich, and F. Kozlowski, "Surface-micromachined electrostatic microrelay," *Sens. Actuators A, Phys.*, vol. 66, no. 1–3, pp. 345–354, Apr. 1998.

[15] J. S. Lee, S. D. Park, A. K. Nallani, G. S. Lee, and J. B. Lee, "Sub-micron metallic electrothermal actuators," *J. Micromech. Microeng.*, vol. 15, no. 2, pp. 322–327, Feb. 2005.

[16] D. A. Fanner and R. A. F. Hammond, "The properties of nickel electrodeposited from a sulphamate bath," *Trans. Inst. Met. Finish.*, vol. 36, pp. 32–42, 1959.

[17] L. S. Stephens, K. W. Kelly, S. Simhadri, A. B. McCandless, and E. I. Meletis, "Mechanical property evaluation and failure analysis of cantilevered LIGA nickel microposts," *J. Microelectromech. Syst.*, vol. 10, no. 3, pp. 347–359, Sep. 2001.

[18] F. Wang, R. Cheng, and X. Li, "MEMS vertical probe cards with ultra densely arrayed metal probes for wafer-level IC testing," *J. Microelectromech. Syst.*, vol. 18, no. 4, pp. 933–941, Aug. 2009.

[19] R. V. Shenoy and M. Datta, "Effect of mask wall angle on shape evolution during through-mask electrochemical micromachining," *J. Electrochem. Soc.*, vol. 143, no. 2, pp. 544–552, 1996.

[20] J. K. Luo, D. P. Chu, A. J. Flewitt, S. M. Spearing, N. A. Fleck, and W. I. Milne, "Uniformity control of Ni thin film microstructure deposited by through-mask plating," *J. Electrochem. Soc.*, vol. 152, no. 1, pp. C36–C41, 2005.

[21] J. K. Luo, A. J. Flewitt, S. M. Spearing, N. A. Fleck, and W. I. Milne, "Comparison of microtweezers based on three lateral thermal actuator configurations," *J. Micromech. Microeng.*, vol. 15, no. 6, pp. 1294–1302, Jun. 2005.

[22] J. K. Luo, A. J. Flewitt, S. M. Spearing, N. A. Fleck, and W. I. Milne, "Three types of planar structure microspring electro-thermal actuators with insulating beam constraint," *J. Micromech. Microeng.*, vol. 15, no. 8, pp. 1527–1535, Aug. 2005.

[23] J. K. Luo, M. Pritschow, A. J. Flewitt, S. M. Spearing, N. A. Fleck, and W. I. Milne, "Effects of process conditions on properties of electroplated Ni thin films for microsystems applications," *J. Electrochem. Soc.*, vol. 153, no. 10, pp. D155–D161, 2005.

[24] E. T. Enikov and K. Lazarov, "PCB-integrated metallic thermal microactuators," *Sens. Actuators A, Phys.*, vol. 105, no. 1, pp. 76–82, Jun. 2003.

[25] R. Hickey, D. Sameoto, T. Hubbard, and M. Kujath, "Time and frequency response of two-arm micromachined thermal actuators," *J. Micromech. Microeng.*, vol. 13, no. 1, pp. 40–46, Jan. 2003.

[26] R. Kickey, M. Kujath, and T. Hubbard, "Heat transfer analysis and optimization of two-beam microelectromechanical thermal actuators," *J. Vac. Sci. Technol. A, Vac. Surf. Films*, vol. 20, no. 3, pp. 971–974, May 2002.

[27] Z. Budrovic, H. V. Swygenhoven, P. M. Derlet, S. V. Petegem, and B. Schmitt, "Plastic deformation with reversible peak broadening in nanocrystalline nickel," *Science*, vol. 304, no. 5668, pp. 273–276, Apr. 2004.

[28] X. Z. Liao, A. R. Kilmametov, R. Z. Valiev, H. Gao, X. Li, A. K. Mukherjee, J. F. Binger, and Y. T. Zhu, "High-pressure torsion-induced grain growth in electrodeposited nanocrystalline Ni," *Appl. Phys. Lett.*, vol. 88, no. 21, p. 021909, May 2006.

[29] G. J. Fan, Y. D. Wang, L. F. Fu, H. Choo, P. K. Liaw, Y. Ren, and N. D. Browning, "Orientation-dependent grain growth in a bulk nanocrystalline alloy during the uniaxial compressive deformation," *Appl. Phys. Lett.*, vol. 88, no. 17, p. 171914, Apr. 2006.

[30] S. C. Chang, J. M. Shieh, B. T. Dai, M. S. Feng, and Y. H. Li, "The effect of plating current density on self-annealing behaviours of electroplated copper film," *J. Electrochem. Soc.*, vol. 149, no. 9, pp. G535–G538, 2002.
[31] W. H. Safranek, "Structure and property relationship for bulk electrodeposits," *J. Vac. Sci. Technol.*, vol. 11, no. 4, pp. 765–770, 1974.

J. K. Luo received the Ph.D. degree from the University of Hokkaido, Japan.

He worked at Cardiff University, U.K., Newport Wafer Fab. Ltd., Philips Semiconductor Company, and Cavendish Kinetics Ltd., Cambridge University. In January 2007, he became a Professor in MEMS at the Centre for Material Research and Innovation (CMRI), University of Bolton, Bolton, U.K. His current research interests focus on microsystems and sensors for biotechnology and healthcare applications, and third generation thin-film solar cells using novel low-cost materials.

Y. Q. Fu received the Ph.D. degree from Nanyang Technological University, Singapore, in 1999.

He was a Research Fellow and Postdoctoral Researcher at Nanyang Technological University, the Singapore–Massachusetts Institute of Technology Alliance, and the University of Cambridge. In September 2007, he joined Heriot-Watt University, Edinburgh, U.K., as a Lecturer on microengineering and bioengineering. His recent research work has focused on microactuators, biosensors, microfluidic devices, and nanotechnology, based on smart functional materials and thin films (such as piezoelectric and shape memory thin films). He has authored or coauthored about 150 refereed international journal papers, one book on thin-film shape memory alloys, and ten book chapters in these areas. He has been regularly invited as a referee for over 30 different international journals, and serves as an editorial board member for three international journals.

J. A. Williams is currently Professor of Engineering Tribology at the University of Cambridge, Cambridge, U.K. He is the author of *Engineering Tribology* and of more than eighty publications. He has held visiting appointments at MIT, the University of New South Wales, and the University of Cape Town.

Prof. Williams is a Fellow of the Institution of Mechanical Engineers, the American Society of Mechanical Engineers, and the Royal Academy of Engineering. He is a past winner of the Tribology Trust Silver Medal.

W. I. Milne received the B.Sc. degree from St. Andrews University, St. Andrews, U.K., in 1970, and the Ph.D. degree in electronic materials from Imperial College London, London, U.K., in 1973 and a DIC in 2003. He was awarded a D.Eng. (*Honoris Causa*) from the University of Waterloo, Waterloo, ON, Canada.

He has been the Head of Electrical Engineering at Cambridge University, Cambridge, U.K., since 1999, Director of the Centre for Advanced Photonics and Electronics(CAPE) since 2004, and Head of the Electronic Devices and Materials group since 1996 when he was appointed to the "1944 Chair in Electrical Engineering." His research interests include large-area Si and carbon-based electronics, thin-film materials and, most recently, MEMS and carbon nanotubes and other 1-D structures for electronic applications. He has published/presented about 650 papers, of which about 150 were invited.

Dr. Milne was elected as Fellow of the Royal Academy of Engineering in 2006 and was awarded the JJ Thomson Medal from the IET in 2008. He is a Guest Professor at HuangZhou University, Wuhan, China, and a Distinguished Visiting Professor at SEU in Nanjing, China, and at NUS, Singapore. He is also a Distinguished Visiting Scholar at KyungHee University, Seoul, Korea.